The Domain Dependence of Chemotaxis in a Two-Dimensional Turbulent Flow

by

Kimberly Jones

A Thesis Presented in Partial Fulfillment
of the Requirements for the Degree
Master of Arts

Approved July 2015 by the
Graduate Supervisory Committee:

Wenbo Tang, Chair
Yun Kang
Donald Jones

ARIZONA STATE UNIVERSITY

August 2015

ABSTRACT

Presented is a study on the chemotaxis reaction process and its relation with flow topology. The effect of coherent structures in turbulent flows is characterized by studying nutrient uptake and the advantage that is received from motile bacteria over other non-motile bacteria. Variability is found to be dependent on the initial location of scalar impurity and can be tied to Lagrangian coherent structures through recent advances in the identification of finite-time transport barriers. Advantage is relatively small for initial nutrient found within high stretching regions of the flow, and nutrient within elliptic structures provide the greatest advantage for motile species. How the flow field and the relevant flow topology lead to such a relation is analyzed.

TABLE OF CONTENTS

LIST OF FIGURES

Chapter 1

INTRODUCTION

Some bacteria, such as E Coli, are able to propel themselves with the use of flagella. These motile species use chemotaxis, a chemical process in which bacteria are able to sense higher concentrations of nutrient and swim up gradient, to gain an advantage on foraging over non-motile species. They are able to reach higher concentrations of food which allows for increased uptake, whereas non-motile species must rely on mixing and diffusion in order to obtain nutrient. This difference in uptake is studied by initializing a localized, high concentration nutrient patch in a sample flow and extracting uptake data over time.

Chemotaxis has been of interest since the late 19^{th} century when Pfeffer first observed the process. Since then, much work has been focused on experiments and modeling to better understand the bacteria behavior. A study by Munoz-Garcia *et al.* (3) showed that advantage is dependent on spatial variability of the nutrient field and diffusivity of the turbulent flow. Recently, Taylor and Stocker (6) have developed a numerical model to simulate chemotaxis in turbulence using a range of physical parameters including chemotactic speed and uptake rate to study advantage of motile bacteria. However, no relevance of the surrounding turbulence was taken into account, and each realization starts with a nutrient patch release in the center of the domain. Turbulence causes transient structures to form and decorrelate, leading to a dependence on the initial starting location of the nutrient patch. The final state of nutrient will be completely homogenized, but there are many stretching and folding patterns which will affect how the nutrient responds in short time.

This thesis seeks to model and study chemotaxis in geostrophic turbulence to gain an understanding of reaction processes in flows. A similar approach to (4) and (5) is taken to explore the transient problem. In those studies, the reaction process is shown to be tied to the Lagrangian topology of the flow as outlined by the finite-time Lyapunov exponents (FTLEs). Haller first proposed the use of FTLE on identification of stretching and attracting structures where he showed that boundaries of coherent structures can be seen as the ridges of the FTLE field (1). Tang and Luna (4) showed reaction rate is intimately connected to Lagrangian stretching history as highlighted by FTLE. Further, a bistable reaction was studied by Tang and Dhumuntarao (5) where convergence to stable states was also linked to FTLE. The previous studies were on advection-reaction-diffusion dynamics where the reaction kinetics exhibit a single or two stable stable equilibria. Here, the variability of reaction due to turbulent mixing is explored further looking at the more complicated dynamics associated with chemotaxis. The flow topology is also related to the more complicated system by means of LCS.

Chapter 2

METHOD

2.1 Governing Equations

Consider a turbulent flow with characteristic length scale L, velocity scale U and viscosity ν. Two species are embedded in the background flow, with equal initial concentration b_0, diffusivity κ and consumption rate ξ. A nutrient is injected into the flow, and one of the bacteria species utilizes chemotaxis to swim up gradient of the nutrient concentration, with a chemotactic speed of χ. The equations for this advection-reaction-diffusion (ARD) system are given in non-dimensional form as

$$c_t + (\boldsymbol{u} \cdot \boldsymbol{\nabla})c = \frac{1}{\mathrm{Pe}}\nabla^2 c - \mathrm{Da}(b+1)c\,, \tag{2.1}$$

$$b_t + (\boldsymbol{u} \cdot \boldsymbol{\nabla})b = \frac{1}{\mathrm{Pe}}\nabla^2 b - \mathrm{Ch}\nabla(b\nabla c)\,, \tag{2.2}$$

where c is the nutrient concentration and b is the concentration of the motile species. The non-motile species is taken to be uniform throughout the simulation with concentration b_0. The background velocity field $\boldsymbol{u}$ advects the scalars. $\mathrm{Pe} = UL/\kappa = \mathrm{Re}\cdot\mathrm{Sc}$ is the Péclet number, where Re is the Reynolds number and $\mathrm{Sc} = \nu/\kappa$ is the Schmidt number. $\mathrm{Da} = \xi b_0 L/U$ is the Damköhler number for bacteria foraging on nutrient and $\mathrm{Ch} = \chi/U$ is the non-dimensional chemotactic speed.

The simulations performed use a length scale L of 6.66 cm and a velocity scale U of 1.5 cm/s. The viscosity ν is set equal to 10^{-6} m^2/sec, with Reynolds number $\mathrm{Re} = 1000$. The diffusivity κ ranges from $10^{-6} \sim 10^{-7}$ m^2/sec, giving a Schmidt number between 1 and 10. A normal Schmidt number for bacteria in the environment

is around 1000, however due to domain size and computational constraints, only the parametric dependence for moderate Sc is explored. The initial concentration for both species is set to 1 and the consumption rate of 0.00225/s is chosen to give a Damköhler number of 0.01. The chemotactic speed is set to $\chi = 1.5$ μm/s with Ch = 0.001. The nutrient is released with an initial Gaussian profile that has peak value 1 and full width at half maximum.

The model is a simplification of the simulations performed in Taylor and Stocker's paper (6). All parameters are consistent with the previous work, with the limited speed restriction removed. A 2D model is considered for better interpretation of physical terms in various flow topology. This makes the analysis more tractable and interpretations can be extrapolated to the higher dimensional case.

To extract scalar information from the simulations, the domain average is defined as the integration over the area

$$\langle q \rangle = \frac{1}{A} \int_D q \, dA \, .$$

The nutrient uptake for motile and non-motile bacteria are respectively given by

$$U_{\mathrm{M}} = \langle b \cdot c \rangle \qquad \text{and} \qquad U_{\mathrm{NM}} = \langle c \cdot 1 \rangle \ .$$

The motility advantage is measured as the difference in uptake of the motile and non-motile species.

2.2 Lagrangian Coherent Structures

Lagrangian Coherent Structures (LCS) are regions of coherent motion in turbulent flows. Finite-time Lyapunov exponents (FTLE) are used to identify locations of

repelling and attracting material lines and surfaces which serve as the boundaries for LCS. To compute the FTLE, let $\mathbf{x}(t; \mathbf{x}_0, t_0)$ denote the current position of a trajectory starting at location $\mathbf{x}_0$, time t_0, and the deformation gradient tensor J as $[\partial \mathbf{x}/\partial \mathbf{x}_0]$. The FTLE field given by

$$\mathrm{FTLE}_{t_0}^{t}(\boldsymbol{x}_0) = \frac{1}{|t - t_0|} \ln \lambda_{\max}(J)\,,$$

is the scalar field which yields the largest stretching rate for any initial position $\boldsymbol{x}_0$, where $\lambda_{\max}(J)$ is the largest eigenvalue of J. In forward time, the FTLE shows regions of repelling surfaces. In backward time, regions of repelling can be seen as attracting surfaces in forward time.

In recent studies (2), it has been pointed out that FTLE ridges can indicate false positives and negatives. Stretching and shear are both highlighted by FTLE, and two closely related quantities, *strainlines* and *shearlines*, are more appropriate features that highlight exponential separation away from material lines. FTLE alone does not highlight transport barriers that enclose elliptic structures; additional methods would be needed when considering these areas. However, FTLE gives a quick way to compute major features of the flow topology, so is it nevertheless used for interpretation here.

2.3 Flow Models

A two dimensional geostrophic turbulence is generated using the vorticity-stream function formulation of an incompressible flow, using direct numerical simulation (DNS). The formulation for the flow is

$$\omega_t + J[\psi, \omega] = d + f, \tag{2.3}$$

where ψ is the stream function of the flow calculated numerically. $\omega = \nabla^2\psi$ is the vorticity. $J[\psi, \omega]$ is the Jacobian matrix. $d = \nabla^2\omega/\mathrm{Re} + \psi$ is the dissipation which includes regular dissipation at small scales and damping at large scales. This prevents inverse energy cascade. f is forcing which ensures conservation of enstrophy at the (2,2) mode. A random phase is added to the forcing, giving emergence and disappearance of coherent structures.

The system is solved using spectral methods for spatial derivatives and a third order Runge-Kutta method for the time step. Periodic boundary conditions are enforced for both dimensions. The flow is integrated until reaching a statistically steady state, from which point the nutrient is introduced and the ARD equations start being solved along with the flow. For Schmidt numbers 1 and 3, a 256 by 256 grid is used to run simulations (realizations for the entire domain are sampled). For higher Schmidt numbers, the resolution is increased to 512 grid points in both direction (only the extreme cases have been analyzed for the higher Schmidt numbers). Note that Schmidt numbers in the realistic environment are on the order of 1000, so more heterogeneity is expected.

Chapter 3

RESULTS

The methods allow for exploration of how variation in chemotactic response is dependent on initial nutrient location within the domain by looking at the flow topology and relation to FTLE.

Fig(3.1) shows the nutrient and motile bacteria concentration for the system where the nutrient was initialized in two distinct regions of the domain. Fig(3.1a) shows a

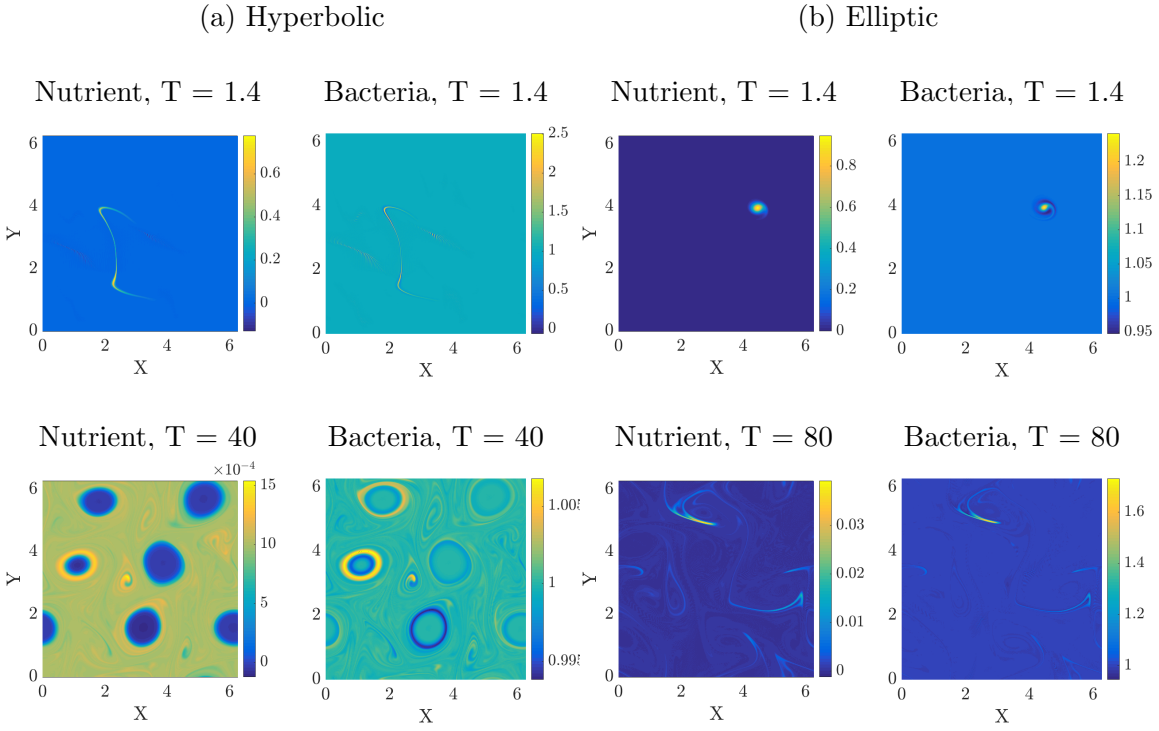

Figure 3.1: A Contrast of Different Stretching Patterns Associated with Patch Release Within Different Flow Coherent Structures. Fig(3.1a) Shows the Nutrient Release and Motile Bacteria Response for a Hyperbolic Release Location. Fig(3.1b) Shows the Scalar Responses with Nutrient Starting in an Elliptic Region, for Which the LCS Boundary Prevents Mixing.

region which has the largest stretching rate, leading to the largest dispersion of nutrient in early time. At a later time, the scalars are shown to homogenize as the nutrient becomes well mixed. In contrast, vortices have transport barriers which prevent large scale mixing outside of the region. At a later time, the nutrient patch evolves outside of the existing elliptic structures because transient vorticies decorrelate. Fig(3.1) emphasizes the difference in release location, showing different stretching of the nutrient. In fig(3.1a), the nutrient stretches out very quickly and shows homogenization in short time. Fig(3.1b) however shows almost no stretching, and at a much later time, the nutrient is still not dispersed. Notice that the motile bacteria have higher concentrations near the nutrient patches. This allows for a larger amount of grazing before the nutrient patch disperses.

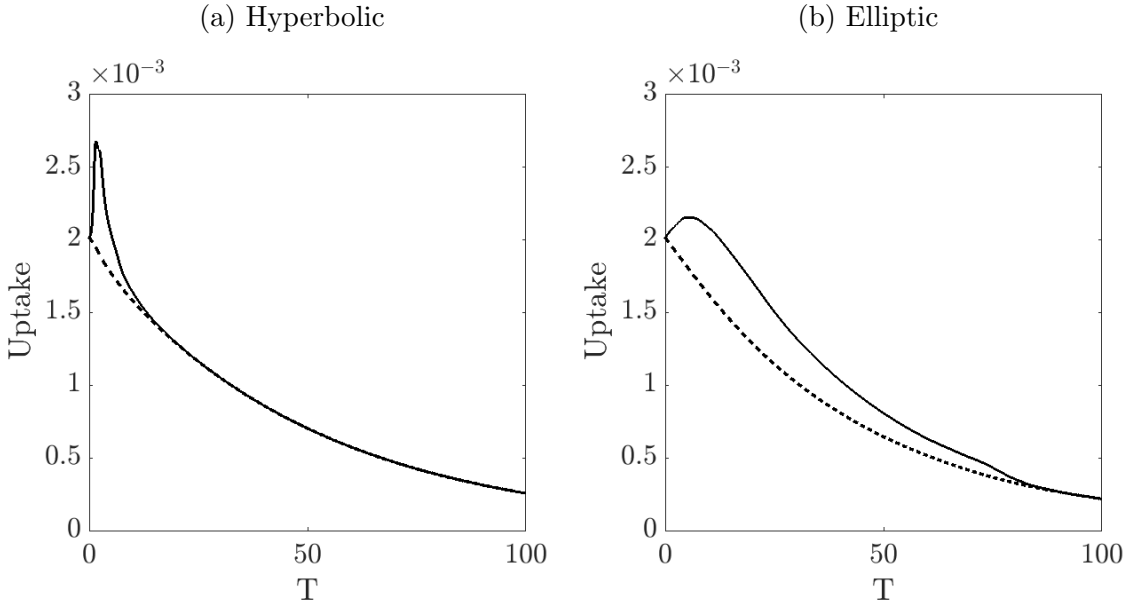

Figure 3.2: Plots of Uptake for Motile and Non-motile Bacteria Based on Hyperbolic and Elliptic Release Locations for Schmidt Number 10. A Solid Line Indicated Motile Species Uptake, with a Dashed Line Representing Non-motile Uptake.

Fig(3.2) shows the uptake for both motile and non-motile species with the nutrient being injected into two regions. When a patch is released in a hyperbolic region

(fig(3.2a)), uptake for motile species peaks and then decays rapidly as mixing causes the nutrient to homogenize. The total uptake advantage for the motile species in this case is 0.015. When the nutrient is initialized in an elliptic region (fig(3.2b)), it takes almost four times as long for the nutrient to become well mixed. The motile species has a greater peak advantage in a hyperbolic release than in an elliptic one, but due to the lack of stretching convergence occurs over a longer time period. It is not until the eddy finally vanishes that the uptake curves converge and the nutrient becomes well mixed. The total uptake advantage when the nutrient is released in an eddy is 0.094, almost an order of magnitude higher than the hyperbolic release. The main advantage for both cases occurs in early time and advantage disappears as nutrient homogenizes. There are clearly distinct behaviors for the different release locations in fig(3.2), showing advantage does indeed depend on starting location, and in fact this dependence can cause significant differences.

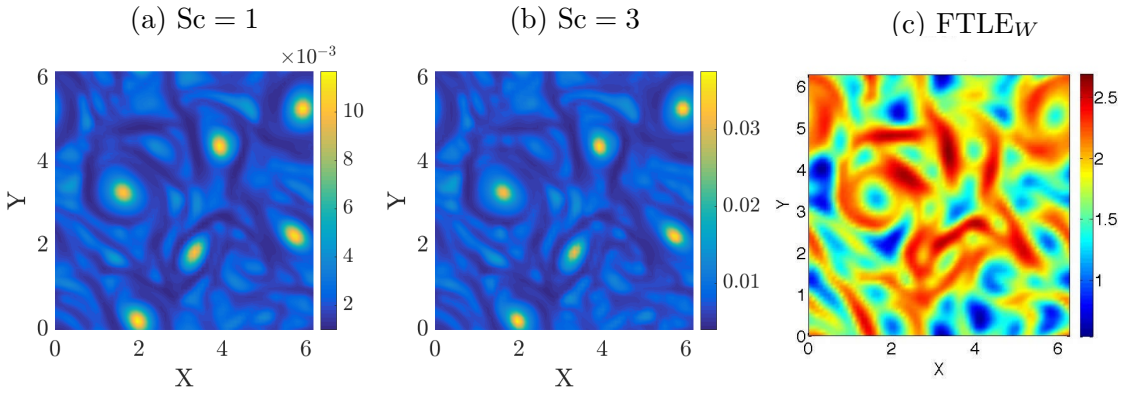

Figure 3.3: Fig(3.3a) and Fig(3.3b) Show Uptake Advantage Based on Release Location for Schmidt Numbers 1 and 3. The Weighted Finite-time Lyapunov Exponent Field Is Shown in Fig(3.3c). The Largest FTLE Values Highlight the Release Locations with Least Advantage.

To explore how the chemotaxis reaction is dependent upon flow topology, simulations were run for Schmidt numbers 1 and 3 based on nutrient release location for

every four points in the domain. The simulations ran for a total of 50 time units, allowing for homogenization of nutrient. The total advantage over the entire domain was extracted for each realization, and then plotted at the corresponding initial release location.

The elliptic regions in fig(3.3a) and fig(3.3b) have the largest total advantage of nutrient over any other starting location due to the lack of transport of nutrient in the domain. On the other hand, the smallest advantage occurs in the regions of greatest stretching. The highest stretching regions of the domain are highlighted as the locations with the largest FTLE values (fig(3.3c)), showing a strong similarity to the release locations which lead to lowest motility advantage. Unfortunately, FTLE does not give a good indication of elliptic regions, so a different detector is needed to locate these structures.

Since each plot requires about 4000 realizations, Schmidt numbers of 1 and 3 were used to save on computation time. A grid resolution four times as dense would be required for higher Schmidt numbers up to 10. Thus, due to time and computational constraints, advantage is not computed for the entire domain for higher Schmidt numbers. Notice from the previous computations in fig(3.2) that greatest and least advantage will occur in elliptic and hyperbolic regions respectively inside the flow domain. It suffices then to run simulations only for these cases at higher Schmidt numbers and look at the variability in advantage.

The range of uptake advantage based on release locations for the entire domain increases with the Schmidt number, as shown in fig(3.4). An increase in gap size as the separation in diffusion and dissipation length scales increases indicates that motility becomes more advantageous with smaller mass diffusivity (fig(3.4a)). The relative advantage (fig(3.4b)) of motile over non-motile species grows with Sc for both elliptic and hyperbolic releases, with elliptic regions increasing at a faster rate than

(a) Difference in Advantage (b) Relative Advantage

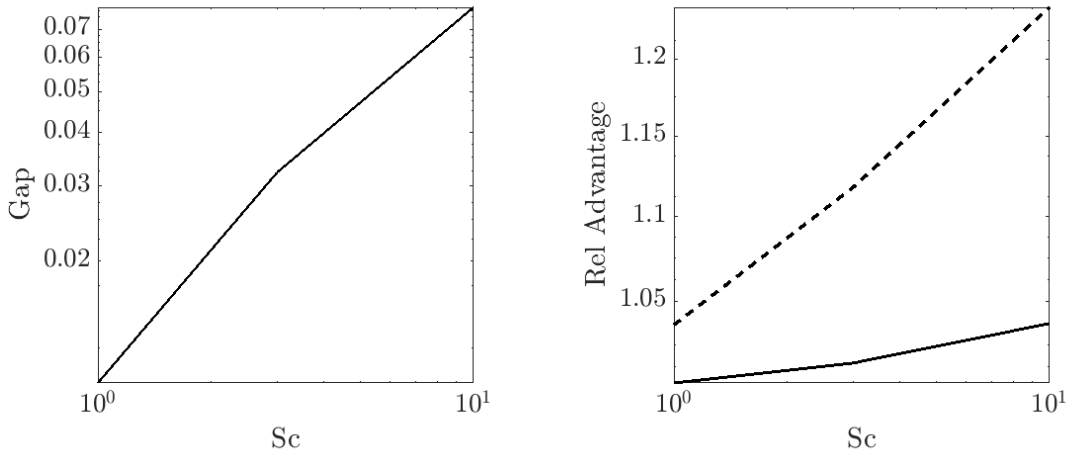

Figure 3.4: Fig(3.4a) Shows the Largest Difference in Advantage for Schmidt Numbers Between 1 and 10. The Relative Advantage Is Shown in Fig(3.4b). The Solid Line Represents Hyperbolic Initialization. Eddy Release Is Shown with the Dashed Line.

hyperbolic regions. For low Schmidt numbers it is clear that the advantage is linearly related to turbulence intensity. Unfortunately, physical turbulence (Sc on the order of 1000) cannot be simulated due to computational constraints.

It is seen in fig(3.3) that the advantage and LCS are tied together with the plot of FTLE. To explore this relationship, a budget is used to determine the variability of the two scalars. The difference between motile and non-motile species concentration is defined to be $w = b - 1$ where b is the concentration of motile bacteria and 1 is its average. Thus w is the fluctuation in motile bacteria concentration over the domain. The new governing equations become

$$c_t + (\boldsymbol{u} \cdot \boldsymbol{\nabla})c = \frac{1}{\mathrm{Pe}}\nabla^2 c - \mathrm{Da}(w+2)c, \tag{3.1}$$

$$w_t + (\boldsymbol{u} \cdot \boldsymbol{\nabla})w = \mathrm{Pe}^{-1}\nabla^2 w - \mathrm{Ch}\nabla[(w+1)\nabla c]. \tag{3.2}$$

The change in variance of c and w over time are found by taking $\langle c \cdot (3.1) \rangle$ and $\langle w \cdot (3.2) \rangle$.

$$\frac{1}{2} \left\langle c^2 \right\rangle_t = -\mathrm{Pe}^{-1} \left\langle |\nabla c|^2 \right\rangle - \mathrm{Da} \left\langle (w+2) c^2 \right\rangle \tag{3.3}$$

$$\frac{1}{2} \left\langle w^2 \right\rangle_t = -\mathrm{Pe}^{-1} \left\langle |\nabla w|^2 \right\rangle - \mathrm{Ch} \left\langle (w+1) \nabla w \nabla c \right\rangle \tag{3.4}$$

The nutrient variance is dependent on dissipation and consumption, while the bacteria variance depends on dissipation and reaction. The change in covariance of the scalars is found by taking $\langle w \cdot (3.1) \rangle + \langle c \cdot (3.2) \rangle$.

$$\langle cw \rangle_t = -2\mathrm{Pe}^{-1} \langle \nabla w \nabla c \rangle - \mathrm{Da} \langle (w+2) cw \rangle + \mathrm{Ch} \left\langle (w+1) |\nabla c|^2 \right\rangle \tag{3.5}$$

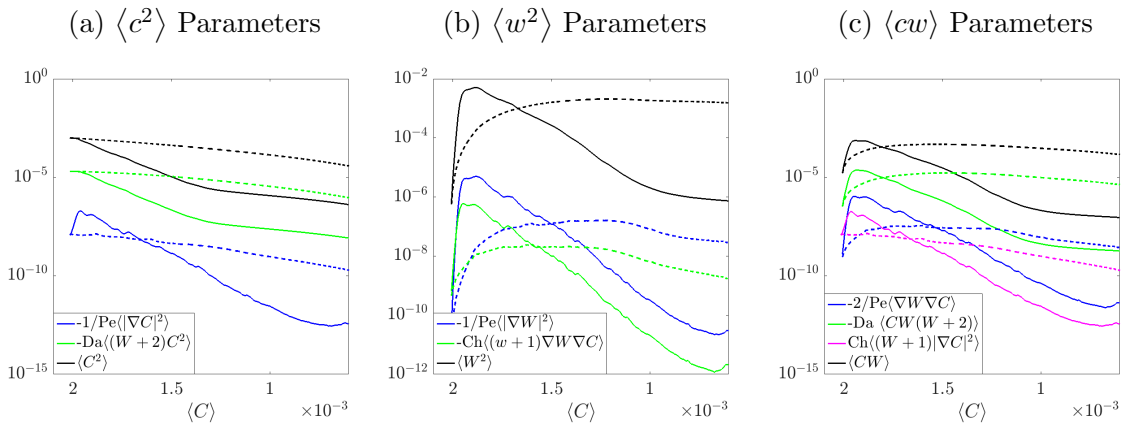

Figure 3.5: Fig(3.5a) Is a Plot of the Variance of Nutrient along with the Two Parameters on the Right Side of Eq. (3.3). Fig(3.5b) Shows the Motile Bacteria Variance and the Parameters given in Eq. (3.4). The Last Plot, Fig(3.5c) Is the Covariance Between the Two Scalars. Also Plotted Are the Terms on the Right Side of Eq. (3.5) Which Contribute to the Change in Variance over Time. $\langle c \rangle$.

As average nutrient concentration decreases, the change in the variance and covariance given by each independent term in Eq. (3.3) and Eq. (3.4) is plotted with the total variance and covariance in fig(3.5). All three figures are plotted against

average concentration. The solid lines indicate hyperbolic initialization, and dashed lines show the case of elliptic region nutrient release (for Sc 10).

Fig(3.5a) plots the variance of nutrient (in black) along with both of the terms on the right hand side of Eq. (3.3). When nutrient is released in an eddy, the variance decreases almost linearly with the average concentration. However, when nutrient is released in a hyperbolic region, the variance exhibits three different phases as average concentration changes. At the highest concentration, the variance decreases at a similar rate to the elliptic release, but quickly begins to decay. As the average concentration decreases, the variance then finally levels off as nutrient is consumed. The blue curve shows the contribution from dissipation, the first term in Eq. (3.3), and the green denotes the second term in Eq. (3.3), the bacterial uptake term. The elliptic realization shows a slow decay which is almost linear for both uptake and dissipation. The hyperbolic uptake term has the same shape as the variance, whereas the dissipation term has three distinct behaviors. There is an increase in early time due to the injection of nutrient. The nutrient then starts to stretch and dissipate giving a steep decay, which finally levels off as the nutrient homogenizes.

The variance of w seen in fig(3.5b) exhibits different behavior. All terms increase in both elliptic and hyperbolic realizations just after the nutrient is released. A hyperbolic release peaks quickly, while an elliptic release slowly plateaus. Notice that the motility term contributes the greatest amount during the initial increase but is quickly superseded by dissipation for both release regions. After the initial increase, the hyperbolic release terms decrease and level off as nutrient homogenizes. The elliptic terms begin to slowly decrease after levelling off.

The covariance terms in fig(3.5c) show similar behaviors. Again, the hyperbolic case has three distinct phases: an increase, decrease, and leveling off, and the eddy release shows a slow increase to a plateau, which slowly decays. The contribution

from the uptake term dominates both other terms over the life of the nutrient patch. Notice that changes in each of the behaviors mentioned above all occur around the same average concentration for each release location.

Chapter 4

CONCLUSION

The dependence on initial conditions was found to have an impact on the uptake advantage for motile bacteria, showing an increase in uptake over non-motile species. Nutrient initialization inside of a high stretching region was shown to provide the least advantage, while elliptic flow structures provide the greatest advantage for motile bacteria with a range of different behaviors between the two extreme cases. There is a large similarity of the advantage gained by release location and LCS, as viewed by the FTLE. The lowest advantages are found in regions of greatest stretching which correspond to the largest values of the FTLE field. A general linear pattern between variability and Schmidt number was also shown, which may allow for scalability to realistic parameters. The plots of variance and covariance showed multiple phases with transitions occurring at the same average concentration. Each phase is tied to distinct dynamical behaviors.

REFERENCES

[1] G. Haller, "Distinguished material surfaces and coherent structures in 3D fluid flows," *Physica D*, **149**, 248–277 (2001).

[2] G. Haller and F. J. Beron-Vera, "Geodesic theory of transport barriers in two-dimensional flows," *Physica D*, **241**, 1680–1702 (2012).

[3] J. Muñoz-Garcia, Z. Neufeld and C. Torney, "Nutrient exposure of chemotactic organisms in small-scale turbulent flows," *New Journal of Physics* **12**, 103043 (2010).

[4] W. Tang and C. Luna, "Dependence of advection-diffusion-reaction on flow coherent structures," *Phys. Fluids*, **25**, 106602, (2013).

[5] W. Tang and A. Dhumuntarao, "Bistability in inhomogeneityEffects of flow coherent structures on the fate of a bistable reaction," *Phys. Fluids*, **27**, 076601, (2015).

[6] J. R. Taylor and R. Stocker, "Trade-offs of chemotactic foraging in turbulent water," *Science*, **338**, 675 (2012).